Desalination and Water Treatment
www.deswater.com

doi: 10.5004/dwt.2019.23947

152 (2019) 99–107
June

A rapid microwave synthesis of nanoscale $BiVO_4/Bi_2O_3@SiO_2$ with large specific surface area and excellent visible-light-driven activity

Xi Zhang[a], Fang-yan Chen[a,b,*], Yu-bin Tang[a,b,*], Yi-ming Liu[a], Xin-gang Wang[a]

[a]*School of Environmental and Chemical Engineering, Jiangsu University of Science and Technology, Zhenjiang Jiangsu, 212003 China, Tel. +86-511-85605157; email: chenfangyan@just.edu.cn (F.-y. Chen), Tel. +86-511-84448601; email: ybbill@163.com (Y.-b. Tang), Tel. +86-511-85605156; emails: 751570182@qq.com (X. Zhang), 694109606@qq.com (Y.-m. Liu), Tel. +86-511-85605157; email: hofs@163.com (X.-g. Wang)*
[b]*Institute of Industrial Technology, Jiangsu University of Science and Technology, Zhangjiagang, 215600 China*

Received 23 August 2018; Accepted 11 February 2019

ABSTRACT

The photocatalyst $BiVO_4/Bi_2O_3@SiO_2$ nanoparticle was synthesized in a high-pressured microwave method. The as-prepared photocatalytst was characterized by X-ray diffraction, scanning electron microscopy, transmission electron microscopy, X-ray photoelectron spectroscopy, UV–Vis diffuse reflectance spectroscopy. The visible-light-driven activity of the prepared photocatalyst was evaluated by degradation of Rhodamine B (RhB). The results show that the as-prepared sample appears in a core-shell structure with the heterojunction $BiVO_4/Bi_2O_3$ as core and amorphous porous SiO_2 as shell. $BiVO_4/Bi_2O_3@SiO_2$ has a large specific surface area (99.63 $m^2\ g^{-1}$) and exhibits superior photocatalytic activity in the degradation of RhB under visible-light illumination. The degradation rate constant of RhB over $BiVO_4/Bi_2O_3@SiO_2$ are 9.8, 9.0, 8.4, and 5.6 times as high as that over Bi_2O_3, $BiVO_4$, $BiVO_4/Bi_2O_3$ and $BiVO_4/SiO_2$, respectively. The enhanced photocatalytic activity of $BiVO_4/Bi_2O_3@SiO_2$ is attributed to both high surface area and low recombination rate of photoinduced electron–hole pairs. The high surface area provides more active sites and superior adsorption properties, which promotes the photocatalytic activity. The low recombination rate of photoinduced electron–hole pairs is due to both the hetero-junction between $BiVO_4$ and Bi_2O_3 and the presence of impurity level of SiO_2.

Keywords: Bismuth vanadate; Bismuth oxide; Silica; Photocatalyst; Microwave; Composites

1. Introduction

Recent years, the utilization of narrow band gap photocatalyst with visible light response for hydrogen evolution and the degradation of organic pollutants have attracted considerable attention [1–5]. $BiVO_4$ is one of the excellent visible-light-driven catalysts due to its superior chemical stability and thermal stability [6]. $BiVO_4$ can exist in three crystal forms such as tetragonal zircon, monoclinic scheelite and tetragonal scheelite. The monoclinic phase bismuth vanadate (*m*-$BiVO_4$) with the narrowest band gap of 2.4 eV has strong response to visible light. So, *m*-$BiVO_4$ has been considered as an effective visible-light-driven photocatalyst for degradation of organics and production of oxygen from water splitting. However, its photocatalytic activity in practical application is inhibited owing to rapid recombination of photoinduced electrons and holes [7]. For this reason, enhancement of the photocatalytic activity of bismuth vanadate has become one of the research hotspots in the field of photocatalyst. Lots of methods, such as morphology control, element doping, exposing active crystal plane, and semiconductor combination has been developed to improve the photocatalytic activity of $BiVO_4$ [8–11]. Of

* Corresponding authors.

these technologies, heterojunction, constructed by combination of two semiconductors with different energy level, can make fast transfer of photoelectrons (or holes) from one semiconductor to another semiconductor. Thus, the recombination of electron–hole pairs is depressed and the photocatalytic activity is improved [12,13]. In recent years, a large number of $BiVO_4$-based heterojunction, such as $BiVO_4$/BiOCl, $AgVO_3$/$BiVO_4$, $BiMoO_6$/$BiVO_4$, and so on, have been synthesized [14–16]. These $BiVO_4$-based heterojunction exhibited, in a way, enhanced photocatalytic activity compared with pure $BiVO_4$.

However, $BiVO_4$-based heterojunction have drawbacks of small specific surface area and poor adsorption performance. Mao et al. [17] have synthesized a porous $BiVO_4$–Bi_2O_3 heterojunction with a specific surface area of only 16.7 m^2 g^{-1}. Wang et al. [18] have synthesized a $BiVO_4$/Bi_2S_3/MoS_2 heterojunction with a specific surface area of only 5.36 m^2 g^{-1}. Zhu et al. [19] have prepared a *p-n* heterojunction $BiVO_4$/TiO_2/GO with a relatively large specific surface area, but only 27.15 m^2 g^{-1}. As known, the specific surface area of the photocatalysts has significant influence on photocatalytic performance. Large surface areas can provide more catalytic activity sites, which can make pollutant molecules adsorbed on the surface of the catalysts for rapid in-situ degradation [20,21]. Therefore, it is meaningful to synthesize bismuth vanadate composites with enriched adsorption-photocatalytic ability.

Recently, microwave-assisted synthesis has been considered as a promising method to synthesize nanoscale inorganic materials due to homogeneous nucleation and shorter crystallization time compared with other conventional heating method. The synthesis of $BiVO_4$ photocatalyst by microwave-assisted method has been reported. Shi et al. [22] have synthesized branched $BiVO_4$ in an atmospheric pressure microwave reactor under conditions of operating power of 800 W and reaction time of 5 h. Mosow and Jothivenkatachalam [23] have synthesized a monoclinic scheelite $BiVO_4$ in a domestic microwave oven under condition of normal pressure. Though microwave-assisted synthesis at ordinary pressure takes shorter time to react than ordinary heating method, still need several hours. It is expected that reaction time will shorten under microwave irradiation at high pressure.

To improve the specific areas of $BiVO_4$-based heterojunction and shorten synthesis time, we present for the first time a microwave-assisted one pot method of a ternary composite $BiVO_4$/Bi_2O_3@SiO_2. $BiVO_4$/Bi_2O_3@SiO_2 was synthesized in a pressure-controllable microwave digestion apparatus, and the reaction time only needs 640 s. Advantage of this method is facile and rapid. In the as-prepared catalyst, $BiVO_4$ and Bi_2O_3 grow in situ to form heterojunction, and porous SiO_2 was coated on the outer layer of the heterojunction to form a core-shell structure. The composite catalyst has a large specific surface area and exhibits excellent adsorption capacity and photocatalytic performance for RhB.

2. Experimental

2.1. Chemicals

Bismuth nitrate pentahydrate, sodium metavanadate, tetraethyl orthosilicate (TEOS), rhodamine B (RhB) and anhydrous ethanol were purchased from Sinopharm Group Chemical Reagent Co., Ltd., China. All reagents were of analytical grade and used as received without further purification.

2.2. Preparation of $BiVO_4$/Bi_2O_3@SiO_2

$Bi(NO_3)_3{\cdot}5H_2O$ (1.94 g) was dissolved in 20 mL of anhydrous ethanol and dispersed by sonication for 20 min, which was marked as solution A. Appropriate amount of $NaVO_3$ was dissolved in 20 mL of absolute ethanol and dispersed by sonication for 20 min to obtain solution B. 1 mL TEOS was dissolved in 20 mL absolute ethanol and stirred for 30 min, and marked as solution C. Under vigorous stirring, solution *B* and solution C were, respectively, added dropwise to solution A, and then 4.5 mL of deionized water was added into the mixed solution, and stirred at 30°C for 1 h to obtain precursor. The precursor was transferred into a 100 mL Teflon-lined autoclave and placed in a pressure-controllable microwave digestion apparatus (XT-9900, Shanghai Xin Tuo Instrument, China) for microwave irradiation for 640 s. The microwave irradiation involved five stages (at stage 1, pressure of 5 kg cm^{-2}, time 90 s; at stage 2, pressure 10 kg cm^{-2}, time 120 s; at stage 3. pressure 15 kg cm^{-2}, time 220 s; at stage 4, pressure 20 kg cm^{-2}, time 130 s; at stage 5, pressure 21 kg cm^{-2}, time 80 s). The resulting yellow product was washed with deionized water and ethanol, dried under vacuum at 65°C for 12 h. Finally, the sample was placed in a muffle furnace and calcined at 450°C with a heating rate of 5°C min^{-1} for 2 h to obtain the desired product. Different amounts of $NaVO_3$ (0.488, 0.287, 0.256, and 0.230 g) were taken to synthesize four samples with Bi/V molar ratios of 1:1, 1.7:1, 1.9:1, and 2.1:1, respectively. The four samples were marked as BVO-S, BVO-BO-S-1.7, BVO-BO-S-1.9, and BVO-BO-S-2.1. Bi/V molar ratio refers to the initial molar ratio of $Bi(NO_3)_3{\cdot}5H_2O$ and $NaVO_3$.

For the sake of comparison, the samples of $BiVO_4$, Bi_2O_3, and composite $BiVO_4$–Bi_2O_3 (BVO–BO) were prepared. $BiVO_4$ and $BiVO_4$–Bi_2O_3 were prepared in the same way as $BiVO_4$-Bi_2O_3-SiO_2 without adding solution C containing TEOS. The Bi/V molar ratios of $BiVO_4$ and $BiVO_4$-Bi_2O_3 were 1.0 and 1.9, respectively. Bi_2O_3 was prepared as follows. $Bi(NO_3)_3{\cdot}5H_2O$ (0.01 mol) was dissolved in 10 mL of 1 mol L^{-1} nitric acid. NaOH (47 mL, 1 mol L^{-1}) was added to the above solution to obtain a white suspension. The suspension was transferred to a 100 mL Teflon-lined autoclave and heated at 150°C for 12 h and then cooled to room temperature. The pale yellow product was washed in turn with ethanol and deionized water, dried at 80°C and subsequently calcined in a muffle furnace at 450°C with heating rate of 5°C min^{-1} for 2 h.

2.3. Characterization of catalysts

X-ray diffraction (XRD) patterns of the photocatalysts were obtained on D8-Advance X-ray diffractometer (Bruker AXS C, Germany) with a Cu–Ka radiation (λ = 1.5406 Å). The morphology and microstructure of the photocatalysts were observed by an S-4800 field emission scanning electron microscope (SEM) (Hitachi, Japan) and a JEM-2100 transmission electron microscope (TEM; Japan Electronics, Japan). UV–Vis diffuse reflectance spectra were collected by a UV-2550 UV-vis spectrophotometer (Shimadzu, Japan)

using $BaSO_4$ as reflectance standard. Elemental composition and chemical valence of the samples were characterized by an ESCALAB-250i X-ray photoelectron spectroscopy (XPS; Thermo Fisher Scientific, USA). The photoluminescence spectra of the photocatalysts were determined by an F4500 fluorescence spectrometer (HITACHI, Japan). The specific surface area was determined by N_2 adsorption–desorption isotherm obtained from Autosorb-1-c sorption analyzer (Quantachrome, USA) and all samples were degassed under a nitrogen atmosphere at 300°C for 10 h, then measured at 77.35 K.

2.4. Electrochemical measurement

Photocurrent measurement was performed on a CHI 660D electrochemical workstation (Chenhua Instrument, China) with a three-electrode cell. Pt wire, saturated Ag/AgCl and FTO electrode deposited with catalyst were used as the counter electrode, reference electrode and working electrode, respectively. Na_2SO_4 aqueous solution (0.1 mol L^{-1}) was employed as electrolyte and 300 W Xe lamp with UV–Vis-cutoff filter ($\lambda > 420$ nm) as the visible-light source.

2.5. Photocatalytic degradation of RhB

The photocatalytic activity of catalyst was evaluated by photocatalytic degradation of RhB. The photocatalyst (50 mg) was dispersed to 100 mL of RhB solution with initial concentration of 5 mg L^{-1} and stirred in the dark for 30 min to ensure adsorption–desorption equilibrium. The suspension was illuminated with visible-light ($\lambda > 420$ nm) emitted from a 300 W Xenon lamp with a 420 nm UV-cutoff filter. 3.5 mL of suspension was taken out at 10 min intervals and centrifuged to remove the photocatalysts, and then the concentration of RhB in the supernatant was determined by UV–Vis spectrophotometer at wavelength of 554 nm. The photodegradation efficiency (E) was calculated by Eq. (1).

$$E = \frac{C_0 - C_t}{C_0} \times 100\% \quad (1)$$

where C_0 (mg L^{-1}) is the initial concentration of RhB, C_t (mg L^{-1}) is the concentration of RhB at time t.

3. Results and discussion

3.1. XRD spectra

Fig. 1 shows the XRD patterns of BVO-S, BVO-BO-S-1.7, BVO-BO-S-1.9, and BVO-BO-S-2.1. The XRD pattern of BVO-S shown in Fig. 1(d) is basically consistent with the standard spectrum of the monoclinic $BiVO_4$ (standard card number JCPDS NO. 14-0688). The peaks at 18.5°, 28.8°, 30.5°, and 35°, correspond to the (011), (121), (040), and (002) crystal planes of the monoclinic $BiVO_4$, respectively [24,25]. Absence of diffraction peaks of Bi_2O_3 in the XRD patterns of BVO-S indicating that the sample BVO-S is a binary composite $BiVO_4/SiO_2$. As seen in the patterns of BVO-BO-S-1.7 (Fig. 1(c)), BVO-BO-S-1.9 (Fig. 1(b)), and BVO-BO-S-2.1 (Fig. 1(a)), diffraction peaks at 18.5°, 28.8°, 30.5°, and 35° belong to monoclinic $BiVO_4$. In addition, peaks at 27.7° and 32.9°are the diffraction peaks of the (201) and (002) crystal planes of the tetragonal phase Bi_2O_3 (standard card number JCPDS NO. 78-1793). It is suggested that as-prepared sample is a ternary composite $BiVO_4/Bi_2O_3/SiO_2$ when the Bi/V molar ratio is more than 1.

The percentage of Bi_2O_3 in composite $BiVO_4/Bi_2O_3$ was in relation to the diffraction peak intensity of Bi_2O_3 (201) and $BiVO_4$ (121) and could be expressed as Eq. (2) [26].

$$Bi_2O_3 \text{ percentage\%} = \frac{I_{Bi_2O_3(201)}}{\left(I_{Bi_2O_3(201)} + I_{BiVO_4(121)}\right)} \quad (2)$$

where I represents the intensity of the diffraction peak.

As shown in the magnified view of the (201) crystal plane of the tetragonal Bi_2O_3 and the (121) crystal plane of the monoclinic $BiVO_4$ (given in the right of Fig. 1), as Bi/V ratio increases, the diffraction intensity of Bi_2O_3 (201) plane becomes stronger, while the diffraction intensity of $BiVO_4$ (121) crystal plane decreases. It is concluded that the Bi_2O_3 content in the sample increases with increasing Bi/V ratio. It is worth mentioning that no diffraction peaks of SiO_2 are found in Fig. 1. It can be deduced that SiO_2 exists in amorphous form [25].

3.2. Morphology

The morphology of $BiVO_4$, BVO-BO-S-1.7, BVO-BO-S-1.9, and BVO-BO-S-2.1 is characterized with SEM and TEM

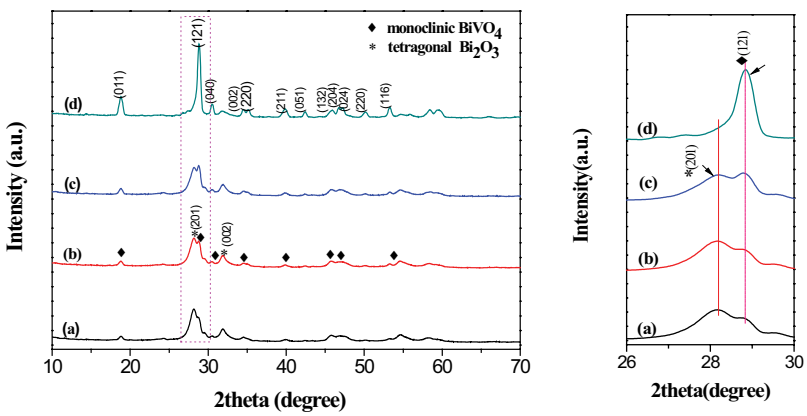

Fig. 1. XRD patterns of BVO-BO-S-2.1 (a), BVO-BO-S-1.9 (b), BVO-BO-S-1.7 (c), BVO-S (d).

shown in Fig. 2. As given in Fig. 2, $BiVO_4/Bi_2O_3@SiO_2$ is nanoparticle with diameter of approximate 50 nm and rough surface.

As seen in TEM image of BVO-BO-S-1.9 (Fig. 2(e)), porously amorphous SiO_2 is coated on the outer layer of the BVO-BO-S-1.9, implying that BVO-BO-S-1.9 has large specific surface area which is beneficial for enhancement of adsorption and consequently photocatalytic activity. Fig. 2(f) shows the high-resolution transmission electron microscopy (HRTEM) image of BVO-BO-S-1.9. The lattice spacing of 0.31 nm corresponds to the (121) crystal plane of $BiVO_4$. The crystal lattice spacing of 0.28 and 0.325 nm correspond to the (002) and (201) planes of Bi_2O_3, respectively. Coexistence of both $BiVO_4$ and Bi_2O_3 phase in hetero-junction region reveals the formation of $BiVO_4/Bi_2O_3$ heterojunction. In a word, the as-prepared BVO-BO-S-1.9 appears to be a core-shell structure with $BiVO_4/Bi_2O_3$ heterojunction as core and porous SiO_2 as shell.

Fig. 3 is the X-ray energy spectrum of BVO-BO-S-1.9. The peaks of the four elements of Bi, V, O, and Si were showed in Fig. 3. Si comes from SiO_2 in the composite and Bi and V come from $BiVO_4$ and Bi_2O_3. O mainly comes from $BiVO_4$, Bi_2O_3, SiO_2 and surface-adsorbed hydroxyl groups. This further proves that the prepared sample BVO-BO-S-1.9 is a ternary complex.

3.3. X-ray photoelectron spectra

Fig. 4 gives the X-ray photoelectron spectra of the BVO-BO-S-1.9. It can be seen from the total spectrum (Fig. 4(a)) that Bi, V, O and Si are found. In high-resolution XPS spectra of Bi element (Fig. 4(b)), the strong peaks at binding energy

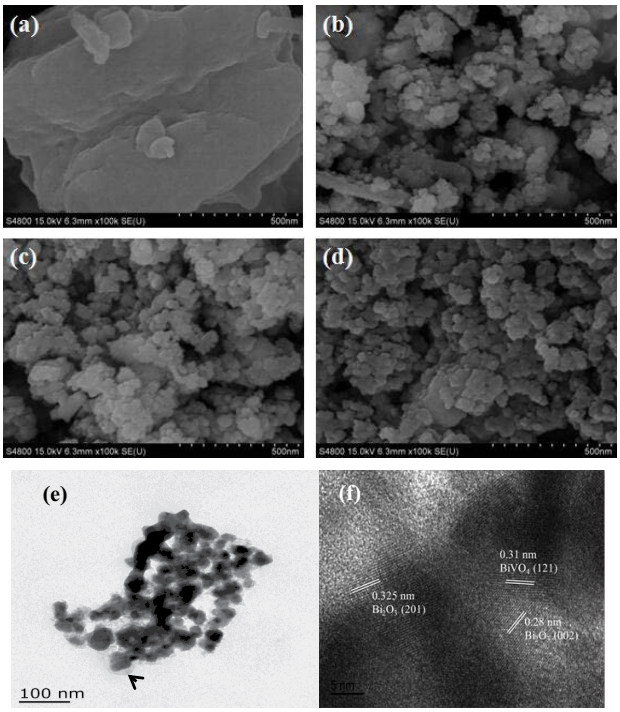

Fig. 2. SEM of $BiVO_4$ (a), BVO-BO-S-1.7 (b), BVO-BO-S-1.9 (c), BVO-BO-S-2.1 (d), TEM (e), HRTEM (f) of BVO-BO-S-1.9.

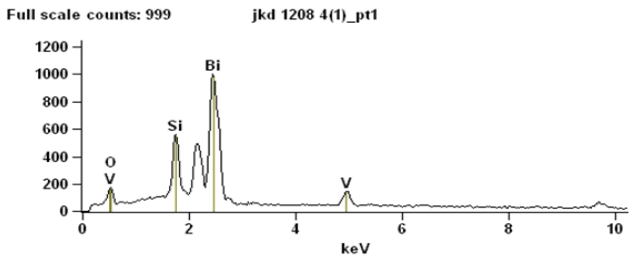

Fig. 3. EDS spectrum of BVO-BO-S-1.9.

of 159.1 and 164.5 eV correspond to Bi 4f7/2 and Bi 4f5/2, respectively. It is demonstrated that Bi is present as Bi^{3+} in the as-prepared photocatalysts [27]. In Fig. 4(c), the binding energy of 524.0 and 516.8 eV are attributed to V 2p1/2 and V 2p3/2, respectively, suggesting the existence of pentavalent vanadium from VO_4^{2-} [15]. As shown in Fig. 4(d), peak of O 1s can be divided into three peaks with binding energy of 530, 532.7, and 533.2 eV, respectively. Of these, the binding energy of 530 eV is assigned to the lattice oxygen of $BiVO_4$ and $Bi_2O_2^{2+}$ [28,29]. The binding energy of 532.7 eV is ascribed to oxygen in Si–O–Si. The binding energy of 533.2 eV is due to the hydroxyl or crystalline water adsorbed on the surface of SiO_2. In high resolution spectrum of Si 2p (Fig. 4(e)), binding energy of 104.14 eV is corresponding to Si in $SiOH_2^+$ [30]. The XPS results further demonstrate the successful synthesis of the ternary composite catalyst containing $BiVO_4$, Bi_2O_3 and SiO_2.

3.4. BET surface area

Fig. 5 shows N_2 adsorption–desorption isotherm and pore size distribution of BVO-BO-S-1.9. As seen in Fig. 5, the isotherm of BVO-BO-S-1.9 is classified as type IV adsorption isotherm according to the Brunauer–Deming–Deming–Teller classification method, suggesting the existence of mesoporous [31]. The Barrett–Joyner–Halenda curve of pore size distribution (inserted in Fig. 5) indicates that most of the pores are in diameter of 2.5–20 nm. This further confirms that SiO_2 coated on the outer layer of $BiVO_4/Bi_2O_3$ is mesoporous. The specific surface areas of the samples are calculated by BET model and listed in Table 1. As given in Table 1, ternary composite $BiVO_4/Bi_2O_3@SiO_2$ has the specific surface area of more than 90 $m^2\ g^{-1}$, which is about four times as large as that of $BiVO_4$. Moreover, the specific surface area increases with increasing of Bi/V ratio.

3.5. UV–Vis diffuse reflectance spectra

Fig. 6(a) gives UV–Vis diffuse reflectance spectra of Bi_2O_3, $BiVO_4$, BVO-S, BVO-BO-S-1.7, BVO-BO-S-1.9, and BVO-BO-S-2.1. As depicted in Fig. 6(a), the absorption edge of $BiVO_4$, Bi_2O_3 and BVO-BO-S-X (X = 1.7, 1.9, and 2.1) is around 540, 460, and 520 nm, respectively, indicating that SiO_2 coated on the outer layers of $BiVO_4$ and $BiVO_4/Bi_2O_3$ heterojunctions has little influence on visible-light response. Nevertheless, in UV-light region, absorption intensity of BVO-BO-S-X (X = 1.7, 1.9, and 2.1) is higher than that of pure $BiVO_4$. This is due to the fact that the presence of porous SiO_2 on outer layer of the ternary composite reduces light reflection and

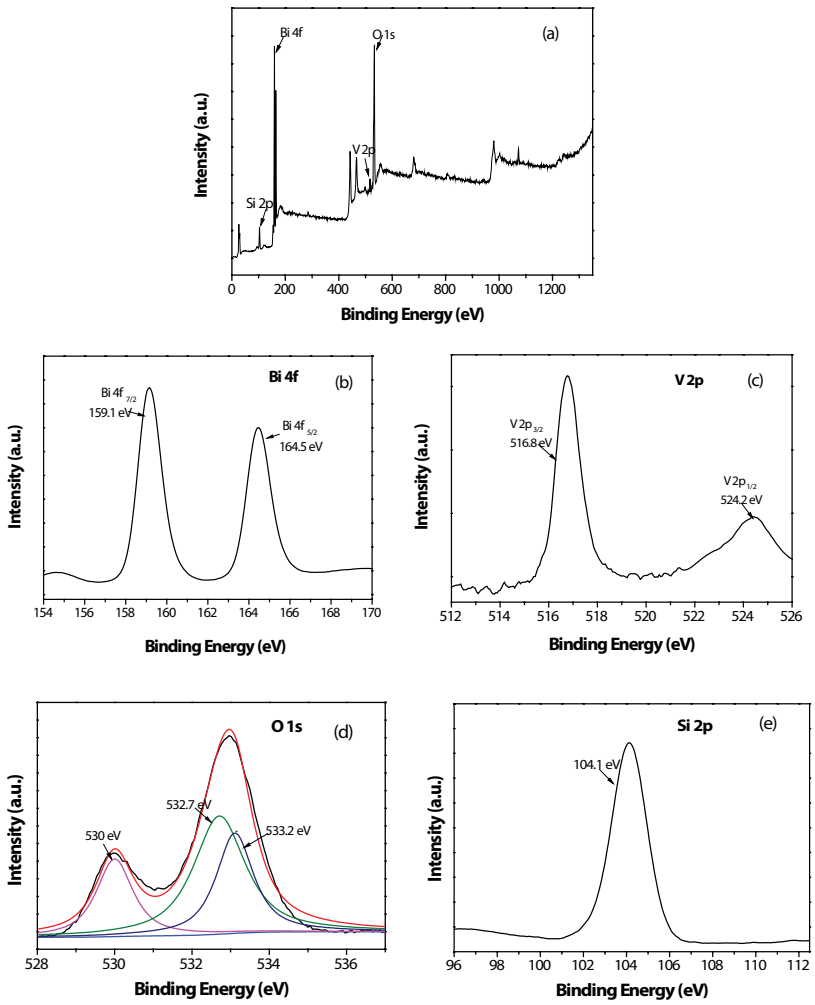

Fig. 4. XPS patterns of BVO-BO-S-1.9.

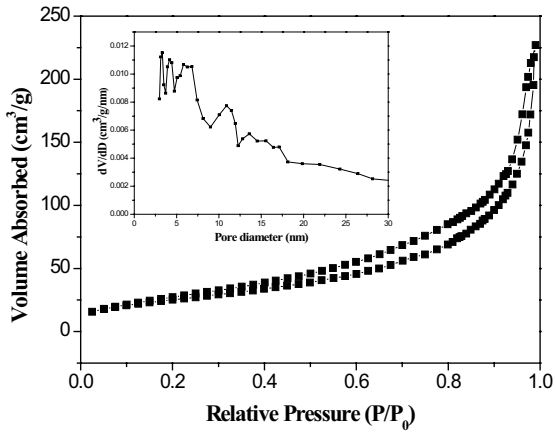

Fig. 5. N_2 adsorption–desorption isotherm and pore-size distribution curve of BVO-BO-S-1.9.

dispersion [32]. Among BVO-BO-S-X (X = 1.7, 1.9, and 2.1), BVO-BO-S-1.9 has the highest light absorption intensity, indicating that it has the best photocatalytic activity.

Table 1
Specific surface area of photocatalysts

Sample	Specific area ($m^2\ g^{-1}$)
$BiVO_4$	14.52
BVO-S	55.37
BVO-BO-S-1.7	91.61
BVO-BO-S-1.9	99.63
BVO-BO-S-2.1	106.86

The band gap (E_g) of a semiconductor photocatalyst can be obtained by Tauc formula expressed as Eq. (3).

$$\alpha h\nu = A\left(h\nu - E_g\right)^{n/2} \tag{3}$$

where α is the absorption coefficient, h is Planck's constant, and ν is the frequency of photons. A is a constant. The value of n depends on the transition characteristics of the semiconductor. Both Bi_2O_3 and $BiVO_4$ are direct band gap semiconductors,

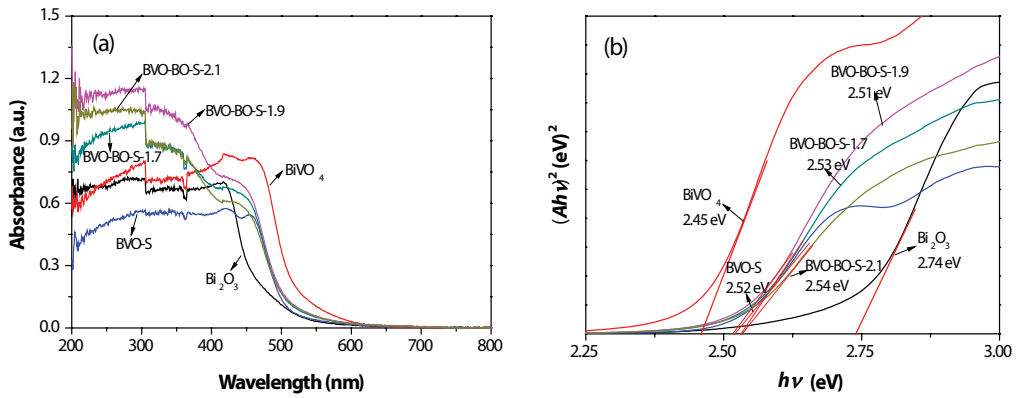

Fig. 6. UV–Vis diffuse reflectance spectra of samples.

the n value is 1 [33]. The plots of $(\alpha h\nu)^2$ vs. $h\nu$ are shown in Fig. 6(b). Thus, the E_g values of Bi_2O_3, $BiVO_4$, BVO-S, BVO-BO-S-1.7, BVO-BO-S-1.9, and BVO-BO-S-2.1 are measured as 2.74, 2.45, 2.52, 2.53, 2.51, and 2.54 eV, respectively. The band gaps of BVO-BO-S-1.7, BVO-BO-S-1.9, and BVO-BO-S-2.1 are less than that of Bi_2O_3 but close to that of $BiVO_4$.

The energy band location of $BiVO_4$ and Bi_2O_3 can be estimated by the Butler equation shown in Eqs. (4) and (5).

$$E_{VB} = X - E^e + 0.5E_g \tag{4}$$

$$E_{CB} = E_{VB} - E_g \tag{5}$$

where E_{VB} is the potential of the valence band (VB), E_{CB} is the conduction band (CB) potential, X is the electronegativity of the semiconductor (the X values of $BiVO_4$ and Bi_2O_3 is 6.04 and 5.95 eV, respectively), and E^e is the free electron energy relative to the hydrogen standard (4.5 eV), E_g is the band gap of the semiconductor [34]. According to Eqs. (4) and (5), the conduction and VB potentials of Bi_2O_3 is calculated as 0.08 and 2.82 eV, respectively; and the conduction and VB potentials of $BiVO_4$ is calculated to be 0.32 and 2.77 eV, respectively.

3.6. Photocatalytic activity

The photocatalytic activity of the samples was evaluated by degradation of RhB under visible-light illumination. The degradation ratios of RhB are presented in Fig. 7(a). As seen from Fig. 7(a), after 60 min of irradiation, the catalytic efficiencies of BVO-BO-S-X (X = 1.7, 1.9, and 2.1) for RhB are 82.7%, 86.7%, and 81.7%, respectively, which are significantly higher than that of Bi_2O_3, $BiVO_4$, BVO-BO, and BVO-S. Moreover, BVO-BO-S-X (X = 1.7, 1.9, and 2.1) exhibits higher adsorption capacity and rapid adsorption rate for RhB than Bi_2O_3, $BiVO_4$, BVO-BO, and BVO-S, which is beneficial for high photocatalytic ability. While the superior adsorption performance of BVO-BO-S-X (X = 1.7, 1.9, and 2.1) originates from larger specific surface area due to the presence of the mesoporous SiO_2 layer on surface of the composite.

The degradation process of RhB can be simulated by the pseudo-first-order kinetic model expressed as Eq. (6) [35] as follows:

$$\ln\frac{C_t}{C_0} = -Kt \tag{6}$$

where C_0 represents the concentration of RhB at the end time of adsorption in the dark, and C_t is the concentration of RhB at t time under visible-light illumination, respectively. K is the apparent rate constant.

As shown in Fig. 7(b), the rate constant of BVO-BO-SX (X = 1.7, 1.9, and 2.1) is obviously higher than that of Bi_2O_3, $BiVO_4$, BVO-BO, and BVO-S. Moreover, the rate constant of BVO-BO-S-1.9 is the highest, which is 9.8, 9.0, 8.4, and

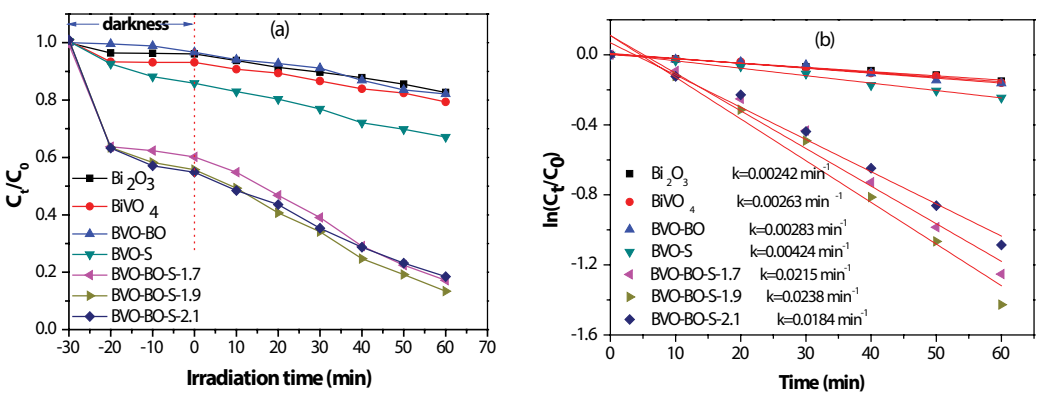

Fig. 7. Photodegradation ratios of RhB under visible-light irradiation.

5.6 times as high as that of Bi_2O_3, $BiVO_4$, BVO-BO, and BVO-S, respectively. Thus, BVO-BO-S-X (X = 1.7, 1.9, and 2.1), especially BVO-BO-S-1.9, is found to exhibit remarkably enhanced photocatalytic ability than Bi_2O_3, $BiVO_4$, BVO-BO, and BVO-S. The enhanced photocatalytic activity of $BiVO_4$/Bi_2O_3@SiO_2 is mainly ascribed to two aspects. One is high surface area and excellent absorption capability due to the presence of porous SiO_2. The other is low recombination rate of photoinduced electron–hole pairs resulting from the heterojunction between $BiVO_4$ and Bi_2O_3.

3.7. Reuse of the photocatalyst

To evaluate the stability of BVO-BO-S-1.9, reuse of BVO-BO-S-1.9 was carried out. As shown in Fig. 8, after being reused for five times, BVO-BO-S-1.9 shows no obviously decreasing activity, indicating that as-prepared photocatalyst is stable and can be reusable.

3.8. Photocatalytic mechanism

3.8.1. Photocurrent response of photocatalysts

To further interpret the higher photocatalytic activity of $BiVO_4$/Bi_2O_3@SiO_2, the charge transfer between $BiVO_4$/Bi_2O_3 and SiO_2 was analyzed by transient photocurrent responses. Fig. 9 gives photocurrent response of $BiVO_4$/Bi_2O_3 (BVO-BO), $BiVO_4$/Bi_2O_3@SiO_2 (BVO-BO-S-1.9), $BiVO_4$/SiO_2 (BVO-S), and $BiVO_4$ for five on–off cycles of intermittent visible light irradiation. Compared with $BiVO_4$/Bi_2O_3, the significantly strong photocurrent response was obtained in the $BiVO_4$/Bi_2O_3@SiO_2, suggesting that the combination of $BiVO_4$/Bi_2O_3 and SiO_2 accelerates the migration of electrons and thus promotes the separation of photoinduced electron–hole pairs [36]. Moreover, photocurrent response of $BiVO_4$/SiO_2 is higher than that of $BiVO_4$. Above results indicate that SiO_2 plays an important role in the electron transfer of $BiVO_4$/Bi_2O_3@SiO_2 and $BiVO_4$/SiO_2. It may because that SiO_2 has defects and impurity levels which can make electrons migrate to SiO_2 surface and thereby inhibit the recombination of photogenerated electron and hole to some extent [37].

3.8.2. Detection of active species

To identify active species produced in photocatalytic degradation of RhB by BVO-BO-1.9. The tripping experiment

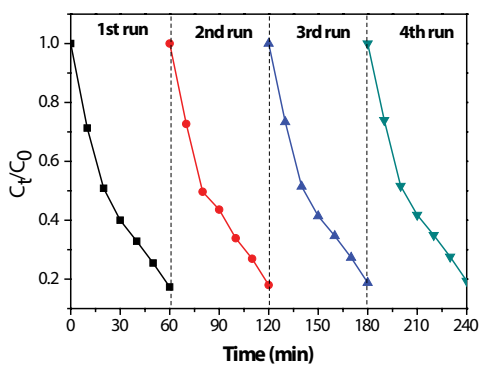

Fig. 8. RhB degradation during the recycle of the BVO-BO-S-1.9.

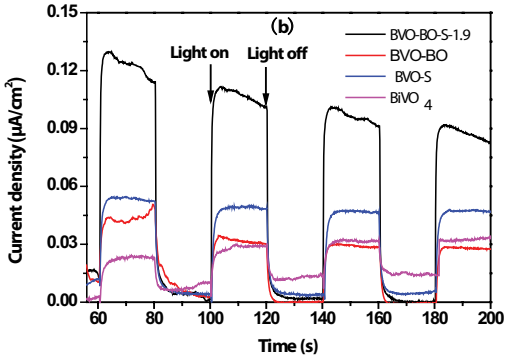

Fig. 9. Transient photocurrent responses of the as-prepared photocatalysts.

of reactive groups was carried out by using *p*-benzoquinone, ethylenediaminetetraacetic acid disodium (EDTA-2Na) and isopropanol as scavengers of superoxide radical ($^{\bullet}O^{2-}$), hole (h^+) and hydroxyl radical ($^{\bullet}OH$), respectively [38]. As shown in Fig. 10, addition of EDTA-2Na during photocatalytic process results in significant decrease in degradation rates, indicating that h^+ is the main active groups for degradation of RhB. Moreover, with introduction of *p*-benzoquinone the degradation rate of RhB decreases to a certain extent, suggesting that $^{\bullet}O^{2-}$ is also involved in degradation of RhB. While $^{\bullet}OH$ plays a little role in photocatalytic reaction.

3.8.3. Proposed mechanism

Based on trapping experiment results, photocurrent measurements and theoretical analysis, the possible mechanism of photoelectron–hole migration and photocatalysis is deduced as shown in Fig. 11. $BiVO_4$ is an intrinsic *n*-type semiconductor whose Fermi level is closer to its CB, and Bi_2O_3 is an intrinsic *p*-type semiconductor whose Fermi level is near to its VB [39]. Therefore, prior to contact, the Fermi level of Bi_2O_3 is lower than that of $BiVO_4$. When two semiconductors are in contact to form *p-n* heterojunction, the diffusion of photogenerated electron–hole pairs between $BiVO_4$ and Bi_2O_3 is enhanced, and then an internal electric field is formed on the interface between $BiVO_4$ and Bi_2O_3 [40]. Meanwhile, the energy band of $BiVO_4$ descend along the Fermi level, while

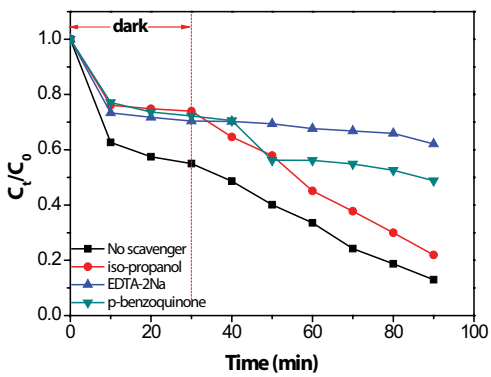

Fig. 10. Photocatalytic degradation of RhB over BVO-BO-S-1.9 in the presence of scavengers.

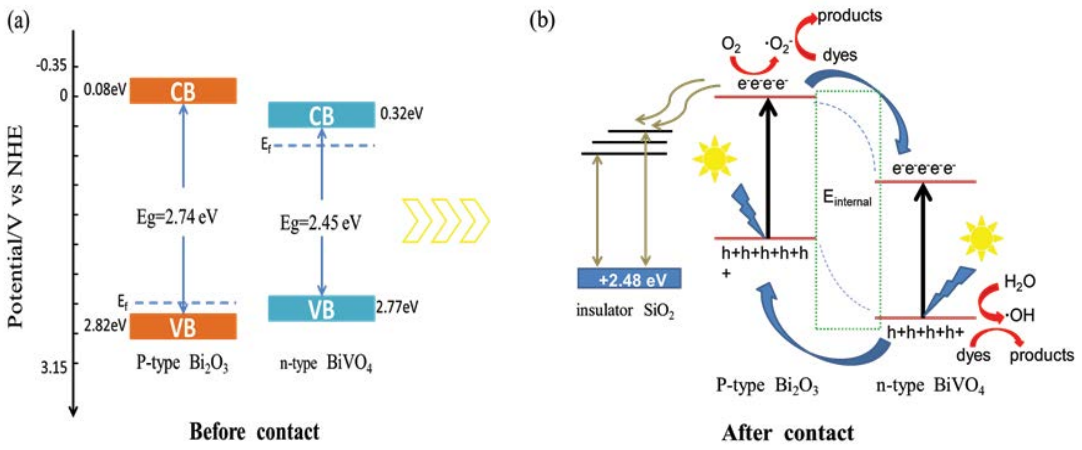

Fig. 11. Schematic illustration of the mechanism for photoinduced electron–hole transfer and photocatalysis.

the energy band of Bi_2O_3 rise along the Fermi level until their Fermi level reaches the same value [41]. Consequently, in the heterojunction $BiVO_4/Bi_2O_3$, the CB and VB of Bi_2O_3 are higher than that of $BiVO_4$, which is depicted in Fig. 11(b). It is noteworthy that SiO_2, as an insulator with band gap of 9 eV, is difficult to be excited to produce photogenerated electron–hole, but the presence of impurity level of SiO_2 has been reported [37]. Hence, the impurity level of SiO_2 is also shown in Fig. 11(b).

As shown in Fig. 11(b), under visible-light (λ > 420 nm) irradiation, photoinduced electrons transfer from the CB of Bi_2O_3 to the CB of $BiVO_4$. Photo-generated holes migrate from the VB of $BiVO_4$ to the VB of Bi_2O_3. Thus, the photoinduced electron–hole of $BiVO_4$ and Bi_2O_3 can be effectively separated. Perhaps, a fraction of electrons on the CB of Bi_2O_3 migrate to the impurity level of SiO_2, which promotes electron–hole separation to some extent [37]. Since the VB potential of $BiVO_4$ is very positive, the holes in the VB can directly oxidize RhB and play the most important role in degradation of RhB. In addition, due to redistribution of charge, the CB potential of Bi_2O_3 is more negative than the standard reduction potential of $O_2/{}^{\bullet}O_2^-$ (−0.33 eV/NHE). Therefore, photogenerated electrons can be trapped by the adsorbed oxygen to generate ${}^{\bullet}O^{2-}$. The produced ${}^{\bullet}O_2^-$ participate in degradation of RhB.

4. Conclusion

A nanoscale photocatalyst $BiVO_4/Bi_2O_3@SiO_2$ was successfully prepared by a one-pot microwave method. The preparation method only requires the use of the necessary precursors bismuth nitrate, sodium metavanadate, TEOS and solvent ethanol without any other auxiliary agents. Under pressured microwave irradiation, the reaction time is only 640 s. Compared with the conventional solvent/water thermal method and atmospheric microwave method, the reaction time is greatly saved.

The as-prepared catalyst appears to be a core-shell structure with $BiVO_4/Bi_2O_3$ heterojunction as core and amorphous porous SiO_2 as shell. $BiVO_4/Bi_2O_3@SiO_2$ exhibits a large specific surface area (99.63 $m^2\ g^{-1}$), excellent adsorption performance and visible-light catalytic activity. It can degrade about 90% of RhB and can be reused. The enhanced photocatalytic activity of $BiVO_4/Bi_2O_3@SiO_2$ is attributed to three aspects. First, the recombination of electron/hole pair is suppressed due to the photoinduced carries transfer on the interface of heterojunction $BiVO_4/Bi_2O_3$. Second, the presence of amorphous porous SiO_2 increases the specific surface area of the composite, thus promoting more pollutant adsorption and providing more active sites. Third, the defects and impurity levels of insulator SiO_2 perhaps make electrons migrate to the SiO_2 surface, thereby, inhibiting the recombination of photogenerated electron and hole to some extent.

Acknowledgement

This work was financially supported by science and technology support projects of Zhangjiagang City, China (No.: ZKS1510).

References

[1] W. Teng, X. Tan, X. Li, Y. Tang, Novel Ag_3PO_4/MoO_3 p-n heterojunction with enhanced photocatalytic activity and stability under visible light irradiation, Appl. Surf. Sci., 409 (2017) 250–260.

[2] Y. Cui, Y. Tang, X. Wang, Template-free synthesis of graphitic carbon nitride hollow spheres for photocatalytic degradation of organic pollutants, Mater. Lett., 161 (2015) 197–200.

[3] H. Wang, C. Yang, M. Li, F. Chen, Y. Cui, Enhanced photocatalytic hydrogen production of restructured B/F codoped g-C_3N_4 via post-thermal treatment, Mater. Lett., 212 (2018) 319–322.

[4] Y. Cui, H. Wang, C. Yang, M. Li, Yi. Zhao, F. Chen, Post-activation of in situ B–F codoped g-C_3N_4 for enhanced photocatalytic H_2 evolution, Appl. Surf. Sci., 441 (2018) 621–630.

[5] Y. Tang, H. Yang, F. Chen, X. Wang, Preparation, characterization of nanocomposites plasmonic photocatalyst C@(Fe_3O_4–halloysite nanotubes)–Ag/AgCl and its photocatalytic activity, Desal. Wat. Treat., 110 (2018) 144–153.

[6] W. Liu, G. Zhao, M. An, L. Chang, Solvothermal synthesis of nanostructured $BiVO_4$ with highly exposed (010) facets and enhanced sunlight-driven photocatalytic properties, Appl. Surf. Sci., 357 (2015) 1053–1063.

[7] S.W. Cao, Z. Yin, J. Barber, F.Y. Boey, S.C. Loo, C. Xue, Preparation of Au-$BiVO_4$ heterogeneous nanostructures as highly efficient visible-light photocatalysts, ACS Appl. Mater. Interfaces, 4 (2012) 418–423.

[8] H.L. Tan, X. Wen, R. Amal, Y.H. Ng, BiVO4 {010} and {110} relative exposure extent: governing factor of surface charge

population and photocatalytic activity, J. Phys. Chem. Lett., 7 (2016) 1400–1405.
[9] J. Zhu, F. Fan, R. Chen, H. An, Z. Feng, C. Li, Direct imaging of highly anisotropic photogenerated Charge separations on different facets of a single $BiVO_4$ photocatalyst, Angew. Chem. Int. Ed., 54 (2015) 9111–9114.
[10] T. Liu, X. Zhou, M. Dupuis, C. Li, The nature of photogenerated charge separation among different crystal facets of $BiVO_4$ studied by density functional theory, Phys. Chem. Chem. Phys., 17 (2015) 23503–23510.
[11] N. Liang, M. Wang, L. Jin, S.S. Huang, W.L. Chen, M. Xu, Q.Q. He, J.T. Zai, N.H. Fang, X.F. Qian, Highly efficient $Ag_2O/Bi_2O_2CO_3$ p-n heterojunction photocatalysts with improved visible-light responsive activity, ACS Appl. Mater. Interfaces, 6 (2014) 11698–11703.
[12] Y. Peng, M. Yan, Q.G. Chen, C.M. Fan, H.Y. Zhou, A.W. Xu, Novel one-dimensional Bi_2O_3–Bi_2WO_6 p-n hierarchical heterojunction with enhanced photocatalytic activity, J. Mater. Chem., 2 (2014) 8517–8524.
[13] X. Lin, D. Xu, S. Jiang, F. Xie, M. Song, H. Zhai, L. Zhao, G. Che, L. Chang, Graphitic carbon nitride nanocrystals decorated $AgVO_3$ nanowires with enhanced visible-light photocatalytic activity, Catal. Commun., 89 (2017) 96–99.
[14] D. Lv, D. Zhang, X. Pu, K. Ding, H. Li, One-pot combustion synthesis of $BiVO_4$/BiOCl composites with enhanced visible-light photocatalytic properties, Sep. Purif. Technol., 174 (2017) 97–103.
[15] R. Wang, L. Cao, Facile synthesis of a novel visible-light-driven $AgVO_3/BiVO_4$ heterojunction photocatalyst and mechanism insight, J. Alloys Compd., 722 (2017) 445–451.
[16] P. Ju, Y. Wang, Y. Sun, D. Zhang, Controllable one-pot synthesis of a nest-like $Bi_2WO_6/BiVO_4$ composite with enhanced photocatalytic antifouling performance under visible light irradiation, Dalton Trans., 45 (2016) 4588–4602.
[17] M. Mao, F. Chen, C. Zheng, J. Ning, Y. Zhong, Y. Hu, Facile synthesis of porous Bi_2O_3-$BiVO_4$ p-n heterojunction composite microrods with highly efficient photocatalytic degradation of phenol, J. Alloys Compd., 688 (2016) 1080–1087.
[18] J. Wang, J. Jin, X. Wang, S. Yang, Y. Zhao, Y. Wu, S. Dong, J. Sun, J. Sun, Facile fabrication of novel $BiVO_4/Bi_2S_3/MoS_2$ n-p heterojunction with enhanced photocatalytic activities towards pollutant degradation under natural sunlight, J. Colloid Interface Sci., 505 (2017) 805–815.
[19] Z. Zhu, Q. Han, D. Yu, J. Sun, B. Liu, A novel p-n heterojunction of $BiVO_4/TiO_2$/GO composite for enhanced visible-light-driven photocatalytic activity, Mater. Lett., 209 (2017) 379–383.
[20] W. Cui, J. He, H. Wang, J. Hu, L. Liu, Y. Liang, Polyaniline hybridization promotes photo-electro-catalytic removal of organic contaminants over 3D network structure of rGH-PANI/TiO_2 hydrogel, Appl. Catal., B, 232 (2018) 232–245.
[21] Y. Zhang, W.Q. Cui, W.J. An, L. Liu, Y. Liang, Y. Zhu, Combination of photoelectrocatalysis and adsorption for removal of bisphenol A over TiO_2-graphene hydrogel with 3D network structure, Appl. Catal., B, 221 (2018) 36–46.
[22] W. Shi, Y. Yan, X. Yan, Microwave-assisted synthesis of nano-scale BiVO4 photocatalysts and their excellent visible-light-driven photocatalytic activity for the degradation of ciprofloxacin, Chem. Eng. J., 215–216 (2013) 740–746.
[23] S. Moscow, K. Jothivenkatachalam, Facile microwave assisted synthesis of floral-shaped $BiVO_4$ nano particles for their photocatalytic and photoelectrochemical performances, J. Mater. Sci. - Mater. Electron., 27 (2015) 1433–1443.
[24] L. Shan, J. Ding, W. Sun, Z. Han, L. Jin, Core–shell hetero-structured $BiVO_4/BiVO_4$: Eu^{3+} with improved photocatalytic activity, J. Inorg. Organomet. Polym Mater., 27 (2017) 1750–1759.
[25] B. Liu, Z. Wang, S. Zhou, J. He, Synthesis and characterization of a novel $BiVO_4/SiO_2$ nanocomposites, Mater. Lett., 160 (2015) 218–221.
[26] O.F. Lopes, K.T.G. Carvalho, W. Avansi, C. Ribeiro, Growth of $BiVO_4$ nanoparticles on a Bi_2O_3 surface: effect of heterojunction formation on visible irradiation-driven catalytic performance, J. Phys. Chem. C, 121 (2017) 13747–13756.
[27] B. zhou, J.H. Qu, X. Zhao, H.J. Liu, Fabrication and photo-electrocatalytic properties of nanocrystalline monoclinic $BiVO_4$ thin-film electrode, J. Environ. Sci., 23 (2011) 151–159.
[28] J. Sun, X. Li, Q. Zhao, M.O. Tade, S. Liu, Construction of p-n heterojunction β-$Bi_2O_3/BiVO_4$ nanocomposite with improved photoinduced charge transfer property and enhanced activity in degradation of *ortho*-dichlorobenzene, Appl. Catal., B, 219 (2017) 259–268.
[29] L. Chen, Q. Zhang, R. Huang, S.F. Yin, S.L. Luo, C.T. Au, Porous peanut-like Bi_2O_3–$BiVO_4$ composites with heterojunctions: one-step synthesis and their photocatalytic properties, Dalton Trans., 41 (2012) 9513–9518.
[30] M. Kaur, R. Malhotra, A. Ali, Tungsten supported Ti/SiO_2 nanoflowers as reusable heterogeneous catalyst for biodiesel production, Renewable Energy, 116 (2018) 109–119.
[31] S. Liu, H. Tang, H. Zhou, G. Dai, W. Wang, Photocatalytic perfermance of sandwich-like $BiVO_4$ sheets by microwave assisted synthesis, Appl. Surf. Sci., 391 (2017) 542–547.
[32] Z. Bai, Y. Hu, S. Yan, W. Shan, C. Wei, Preparation of mesoporous $SiO_2/Bi_2O_3/TiO_2$ superhydrophilic thin films and their surface self-cleaning properties, RSC Adv., 7 (2017) 1966–1974.
[33] Z. Lin, W. Wang, S. Liu, L. Zhang, H. Xu, A sonochemical route to visible-light-driven high-activity $BiVO_4$ photocatalyst, J. Mol. Catal. A: Chem., 252 (2006) 120–124.
[34] S.R. Zhu, Q. Qi, W.N. Zhao, Y. Fang, L. Han, Enhanced photocatalytic activity in hybrid composite combined BiOBr nanosheets and Bi_2S_3, nanoparticles, J. Phys. Chem. Solids, 121 (2018) 163–171.
[35] S.R. Zhu, M.K. Wu, W.N. Zhao, F.Y. Yi, K. Tao, L. Han, Fabrication of heterostructured BiOBr/$Bi_{24}O_{31}Br_{10}/TiO_2$ photocatalyst by pyrolysis of MOF composite for dye degradation, J. Solid State Chem., 255 (2017) 17–26.
[36] M.Y. Li, Y.B. Tang, W.L. Shi, F.Y. Chen, Y. Shi, H.C. Gu, Design of visible-light-response core–shell $Fe_2O_3/CuBi_2O_4$ heterojunctions with enhanced photocatalytic activity towards the degradation of tetracycline: Z-scheme photocatalytic mechanism insight, Inorg. Chem. Front., 5 (2018) 3148–3154.
[37] Q. Hao, X. Niu, C. Nie, S. Hao, W. Zou, J. Ge, D. Chen, W. Yao, A highly efficient g-C_3N_4/SiO_2 heterojunction: the role of SiO_2 in the enhancement of visible light photocatalytic activity, Phys. Chem. Chem. Phys., 18 (2016) 31410–31418.
[38] Y. Fu, X. Sun, W. Xin, $BiVO_4$–graphene catalyst and its high photocatalytic performance under visible light irradiation, Mater. Chem. Phys., 131 (2011) 325–330.
[39] G. Zhu, Y. Liu, M. Hojamberdiev, J. Han, J. Rodriguez, S.A. Bilmes, P. Liu, Thermodecomposition synthesis of porous β-$Bi_2O_3/Bi_2O_2CO_3$ heterostructured photocatalysts with improved visible light photocatalytic activity, New J. Chem., 39 (2015) 9557–9568.
[40] H. Wu, X. Ding, W. Li, C. Ren, H. Yang, PVP-assisted synthesis and photocatalytic properties of magnetic Fe_3O_4/SiO_2/BiOBr composite, J. Mater. Sci. - Mater. Electron., 28 (2017) 18542–18550.
[41] Y. Cheng, H. Wang, Y. Zhu, F. Liao, Z. Li, J. Li, One-step hydrothermal synthesis of $BiVO_4$-Bi_2O_3 p-n heterojunction composites and their enhanced photocatalysis properties, J. Mater. Sci. - Mater. Electron., 26 (2015) 1268–1274.